Organic & Biomolecular Chemistry

Cite this: *Org. Biomol. Chem.*, 2012, **10**, 5366

www.rsc.org/obc

PAPER

A cyanine based fluorophore emitting both single photon near-infrared fluorescence and two-photon deep red fluorescence in aqueous solution†

Lu Wang,‡[a] Jiefu Jin,‡[b] Xishan Chen,[a] Hai-Hua Fan,[c] Billy King Fai Li,[c] Kok-Wai Cheah,[c] Ning Ding,[a] Shenghong Ju,*[d] Wing-Tak Wong*[e] and Cong Li*[a]

Received 26th March 2012, Accepted 30th May 2012
DOI: 10.1039/c2ob25619c

Optical imaging provides an indispensable way to locate tumors in their early stages with high sensitivity and signal to background ratio. A heptamethine cyanine based fluorophore that emits both single photon near-infrared fluorescence and two-photon deep red fluorescence under physiological conditions was developed. Linear and nonlinear photophysical properties of this fluorophore were investigated and it demonstrated the capability to label lysosomes in cancer cells. The advantages of this fluorophore, including tolerable cytotoxicity, high fluorescence quantum yield, and the ability to emit both near-infrared single photon fluorescence and deep red two photon fluorescence in aqueous solution, give it potential to be used in intra-operatively optical image-guided tumor excision followed by two-photon fluorescence microscopy biopsy analysis after a single administration.

Introduction

Surgery is a primary treatment strategy for most solid tumors. The completeness of tumor removal during surgery is usually considered of the most importance to achieve a satisfactory prognosis.[1] Currently, the differentiation of neoplastic tissue from normal tissue relies on the surgeon's ability and experience based on subjective criteria that are not easily quantifiable. However, the absence of a clear and distinctive boundary of malignant tumor combined with the lack of a screening tool often results in a compromised therapeutic response.[2,3] For example, due to the heterogeneous and infiltrative nature, it is very difficult to precisely delineate the margin of a malignant brain tumor, which results in a median survival of below 15 months for patients.[4] Therefore, any improvements in complete tumor removal will benefit the therapeutic efficacy for cancer patients.

Image-guided surgery is the most promising way to remove the neoplastic tissue while minimizing the damage to the neighboring normal tissues.[5,6] Among numerous imaging modalities, fluorescence-based optical imaging affords advantages in intra-operative tumor resection due to its superior sensitivity, non-ionized radiation, short acquisition time and convenience for manipulation.[7] Tsien *et al.* developed a matrix metalloproteinase (MMP) responsive fluorescence probe to guide tumor excision during surgery.[8] The experimental results showed that animals whose tumors were resected under image guidance had better long-term survival than animals whose tumors were resected with traditional bright-field illumination.[1] Most recently, Ntziachristos *et al.* for the first time demonstrated the feasibility of optical imaging guided tumor resection in humans.[2] After intravenous injection of a fluorecein labeled folic acid to ovarian cancer patients, tumors with a diameter as low as 1.0 mm can be clearly identified and excised completely. All the excised tissues were confirmed to be malignant by histopathological analysis.

The key step to advance the clinical translation of optical image-guided surgery is the development of a probe with higher sensitivity, targeting specificity and lower toxicity.[9,10] Compared to fluorescein with visible green fluorescence, probes that absorb and emit in a wavelength range from deep red to near-infrared (NIR) (650–950 nm) attract much attention because absorbance and autofluorescence of tissues in this range are low, which benefits the visualization of lesions with high sensitivity and

[a]*Key Laboratory of Smart Drug Delivery, Ministry of Education & PLA, School of Pharmacy, Fudan University, Shanghai 201203, China. E-mail: congli@fudan.edu.cn; Fax: +86 21 5198 0100; Tel: +86 21 5198 0100*
[b]*Department of Chemistry, The University of Hong Kong, Pokfulam Road, Hong Kong*
[c]*Centre of Advanced Luminescence Materials, Department of Physics, Hong Kong Baptist University, Kowloon Tong, Hong Kong, China*
[d]*Jiangsu Key Laboratory of Molecular and Functional Imaging, Department of Radiology, Zhongda Hospital, Medical School, Southeast University, Nanjing 210009, China. E-mail: jsh0836@hotmail.com; Fax: +86 25 8327 2121; Tel: +86 25 8331 1083*
[e]*Department of Applied Biology and Chemical Technology, The Hong Kong Polytechnic University Shenzhen Research Institute, The Hong Kong Polytechnic University, Hunghom, Kowloon, Hong Kong. E-mail: bcwtwong@polyu.edu.hk; Fax: +852 2364 9932; Tel: +852 3440 8789*

†Electronic supplementary information (ESI) available: Detailed synthesis and characterization of the fluorophores, photospectroscopy of **1a–1c**, *in vitro* cytotoxicity, SP and TP fluorescence microscopic studies, Fig. S1–S4, NMR and MS spectra. See DOI: 10.1039/c2ob25619c

‡These authors contributed equally to this work.

target to background signal ratio.[11,12] Additionally, suspected neoplastic tissues showing high fluorescence during image-guided surgery need to be pathologically verified. Fluorescence microscopy is not only helpful to identify the pathological status of excised tissues, but also useful to delineate the boundary between the neoplastic and normal tissues with a spatial resolution at a sub-micrometer scale.[13] Compared to traditional single-photon fluorescence microscopy (SPFM), two-photon fluorescence microscopy (TPFM) shows deeper penetration depth (>500 μm), lower tissue auto-fluorescence and self-absorption, reduced photodamage and photobleaching, which allows imaging of deep loci embedded in the tissue sample for a long period of time without signal attenuation.[14] Therefore, a fluorophore that emits both single photon (SP) NIR fluorescence and two-photon (TP) deep red fluorescence will provide great convenience for optical image-guided tumor excision followed by biopsy examination.

Results and discussion

Design and synthesis of the fluorophores

In this work, heptamethine cyanine derivatives were chosen as a prototype of the dual functional fluorophores because of their high extinction coefficient and optimal emission wavelength.[15] For example, indocyanine green (ICG) has been approved by FDA as a diagnostic medicine to determine cardiac output, hepatic function, liver blood flow, and ophthalmic angiography for over 30 years with an excellent safety record.[16] Heptamethine cyanine based NIR fluorophores and their derivatives have been extensively investigated to image pH,[17] inorganic ions,[18] endogenous reactive nitrogen species,[19] oxidative stress[20] and protease activity.[21] Previous reports showed that substituents at the 5-position of the indole ring can mediate the optical properties of heptamethine cyanine derivatives.[22] Meanwhile, photophysical properties of cyanine derivatives were also closely related to their aggregation states in aqueous solution, which depends on their charge density, hydrophilicity and polarity.[23] Bearing these in mind, six cyanine derivatives including IR783, a well-known NIR fluorophore were prepared, in which the 5-position of the indole ring was functionalized with proton, methyl as an electron-donor group or chloride as an electron-withdrawing group. Meanwhile, sulfate or carboxylic acid was modified at the *N*-alkylated carbon chain terminals to adjust the charge density and hydrophilicity of the resulting fluorophores. Additionally, the modified carboxylic acids provide convenience to label the fluorophore with biomacromolecules such as antibodies through an amide bond to achieve the targeted imaging purpose.

All heptamethine cyanine derivatives were synthesized from corresponding alkylated indolium salts using a stepwise process developed by Waggoner and co-workers.[24] As shown in Scheme 1, treatment of 5-substitited-2,3,3-trimethyl-3*H*-indolium with 5-bromovaleric acid or 1,4-butane sultone in *o*-dichlorobenzene gave the corresponding *N*-alkylated indolium derivatives **4a–c** functionalized with carboxylic acid or **5a–c** functionalized with sulfate. Meanwhile, the reaction between cyclohexanone with phosphorus oxychloride ($POCl_3$) in the presence of *N*,*N*-dimethylformamide (DMF) offered

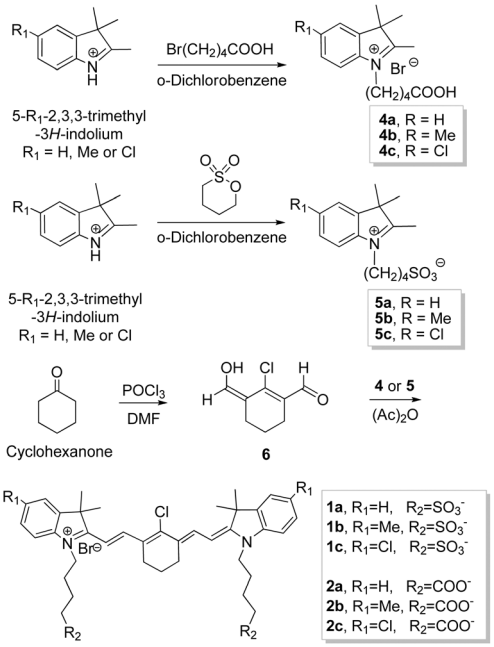

Scheme 1 General synthetic procedure for the cyanine based fluorophores.

Table 1 Photophysical parameters of fluorophores in PBS (pH 7.4)

Dye	$A_{max\ SP}$ (nm)[a]	$\varepsilon_{max\ SP}$ (cm^{-1} mol^{-1})[b]	$\lambda_{max\ SP\ (TP)}$ (nm)[c]	Φ_{SP}[d]/$_{TP}$[e] (%)	σ_{TP}[f]
1a	775	120 000	797 (n.d.)	6.5/0.033	2.71
2a	775	56 000	796 (642)	30/0.982	33.9
1b	787	61 500	808 (656)	8.5/0.747	10.4
2b	788	38 200	807 (n.d.)	7.5/0.845	0.538
1c	791	49 800	806 (n.d.)	1.2/0.0833	1.30
2c	789	16 900	807 (n.d.)	13/1.28	0.389

[a] Maximum absorbance wavelength of fluorophores. [b] Extinction coefficients at A_{max}. [c] Maximum SP and TP emission wavelength. [d] Quantum yields (QY) of the fluorophores correlated to ICG. [e] QYs of two-photon fluorescence of the fluorophores referenced to Rhodamine 6G (λ_{ex} = 450 nm, QY_{R6G} = 95% in MeOH). [f] Two-photon absorption cross section of fluorophores (10^{-4} M) at λ_{ex} = 900 nm referenced to R6G (σ_{R6G} = 2.1 GM, 1 GM = 10^{-50} cm^4 s $photon^{-1}$ $molecule^{-1}$).

cyclohexanecarboxaldehyde **6**, which condensed with **4a–c** or **5a–c** to give the target heptamethine cyanines **1a–c** or **2a–c** with yields in a range of 72–90%. During the final condensation step, addition of **6** to *N*-alkylated indolium in acetic anhydride dropwise substantially increased the yield of resulting cyanines. Due to the unstable aldehyde groups at high temperature, addition of **6** in batches may minimize its unwanted decomposition during the reaction.

Absorbance and SP fluorescence studies in aqueous solution

The photophysical properties of the six fluorophores were investigated in phosphate buffered saline (PBS) at pH 7.4 and the corresponding photospectroscopic parameters are listed in Table 1. It is obvious that the substituents at the indole rings and

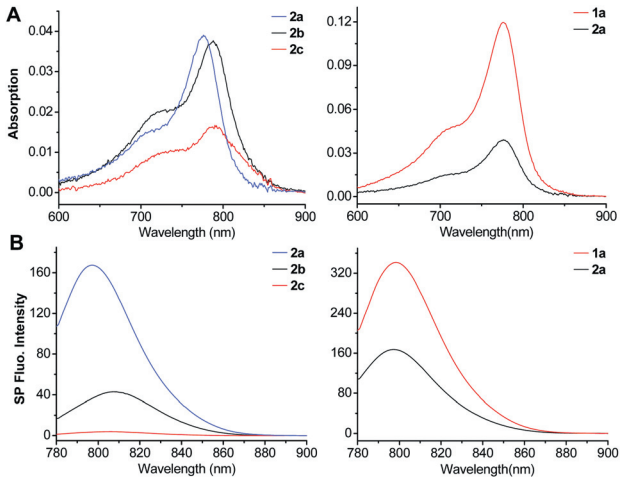

Fig. 1 Substituents at the indole ring and *N*-alkylated carbon chain terminals significantly affect the absorbance and emission of the fluorophores in PBS (pH 7.4). (A) Absorbance of **2a–2c** (1.0 μM, left panel) with different substituents at indole ring and absorbance of **1a–2a** (1.0 μM, right panel) with different groups at carbon chain terminals. (B) SP fluorescence spectra of **2a–2c** (1.0 μM, left panel) and **1a–2a** (1.0 μM, right panel) after excitation at 765 nm.

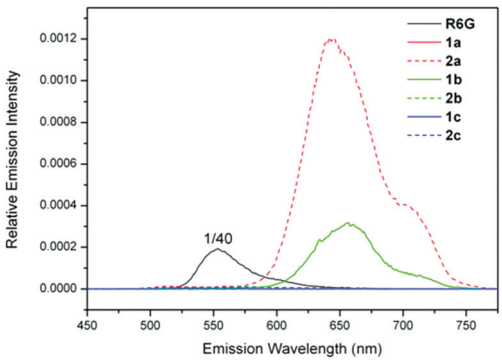

Fig. 2 TP fluorescence spectra of **1a–1c**, **2a–2c** and rhodamine (100 μM) after excitation at 900 nm in PBS (pH 7.4). The spectrum of rhodamine was minimized 40 times to fit with the other fluorophores. Fluorophores **2a** and **1b** demonstrated remarkable TP fluorescence in PBS.

N-alkylated carbon chain terminals significantly change absorbance and emission spectra of the fluorophores. Fig. 1A demonstrates the absorbance of **2a–c** with different substituents at indole ring (left panel) and absorbance of **1a–2a** with different functional groups at *N*-alkylated carbon chain terminals (right panel). Substitution of either an electron donating or electron withdrawing group at the indole ring led to a red-shift of the absorbance. This phenomenon can be explained by the participation of the lone pair electrons or σ-electrons of the substituents in the big-π conjugation system of cyanine, which leads to the decrease of the electron transition energy level. Notably, the replacement of sulfates by carboxylate acid at *N*-alkylated carbon chain terminals did not lead to any shape variation or position movement of the absorbance, which implies these groups do not belong to the chromophore system. Remarkably, the extinction coefficient of **2a** decreased 53% compared to **1a** (Table 1). The functionalization of the carboxylic acid may decrease the polarity and negative charge of fluorophore in aqueous solution, which increases the self-aggregation tendency of the fluorophores and results in the decrease of extinction coefficient. Fig. 1B showed SP emission spectra of **2a–c** (left panel) and **1a–2a** (right panel) in PBS. Substitution of chloride on the indole ring greatly reduced the fluorescence intensity. For example, SP fluorescence of **1c** and **2c** in PBS were measured as only 4.4% and 2.1% compared to that of **1a** and **2a** (Fig. 1B and S1†). The above chloride dominated quenching effect may be attributed to the internal heavy atom effect, in which the attachment of a halogen atom on the indole ring enhances the spin–orbit perturbation in the fluorophore and accelerates the intercombination transition through a S1–T1 spin-forbidden process.[25] Unexpectedly, replacement of the sulfates with carboxylate acid at the carbon chain terminal results in substantial enhancement of quantum yield (Q.Y.). For example, the Q.Y. of **2a** and **2c** increased 4.6 and 10.8 times compared to those of **1a** and **1c** (Fig. S2†). The decreased hydrophilicity and charge density of the fluorophores after modification with carboxylate acids may disturb the structure of H-type aggregates that are well-documented for their non-emissive characteristics in the aqueous solution.[23,26]

TP fluorescence studies in aqueous solution

Nonlinear photophysical properties of the fluorophores were investigated in PBS under TP excitation provided by a femtosecond mode-locked Ti:sapphire laser system. In all six fluorophores, only **2a** and **1b** demonstrated remarkable TP absorption cross section values of 33.9 and 10.4 GM (1 GM = 10^{-50} cm^4 s $photon^{-1}$) at 900 nm (Table 1). Interestingly, compared with **1a**, the replacement of sulfates by carboxylate acid endows **2a** with 30 and 13 time enhancements in TP induced fluorescence QY (Φ_{TP}) and TP absorption cross section (σ_{TP}). Consistent with the above data, **2a** and **1b** demonstrated comparable TP induced fluorescence intensities compared to Rhodamine 6G (R6G) upon excitation at 900 nm (Fig. 2). Importantly, the power-dependence fluorescence curve of **2a** (Fig. S3†) indicated the fitting exponent of input power to be 1.8655, implying that 900 nm fs-pulsed incident light indeed initiated a TP absorption process in **2a**. Recently, Achilefu *et al.* reported heptamethine cyanine derivatives such as cypate demonstrating high TP action cross-section and prolonged fluorescence lifetime.[27] 1550 nm was chosen as the TP excitation wavelength because cypate demonstrated its maximum absorbance at 750–800 nm, which benefits the generation of strong TP fluorescence in the NIR window. In this work, the fluorophores were excited at 900 nm instead of 1550 nm to generate TP fluorescence that can be visualized by the naked eye. In this way, the emission not only possesses the inherent advantages of TP fluorescence, but also provides great convenience to distinguish the neoplastic tissue from surrounding normal tissues for the surgeons. **2a** demonstrated an obvious absorbance at 440–500 nm that is a prerequisite to produce the strong deep red TP fluorescence after excitation at 900 nm. Compared to the reported TP fluorophores such as DTTC and cypate,[28] **2a** showed additional advantages including high water solubility and uncompromised TP fluorescence in aqueous

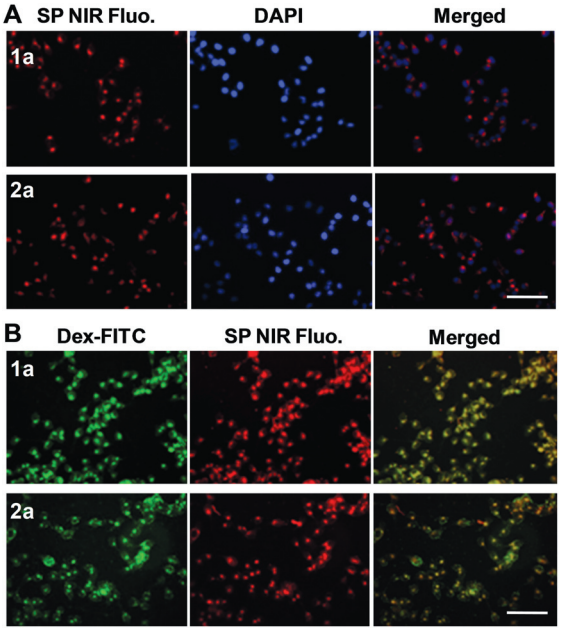

Fig. 3 Cyanine based fluorophores demonstrated the capabilities to label lysosomes in HeLa cells. (A) SPFM images of cells at 24 h post-incubation with **1a** (1.0 μM, upper panel) or **2a** (lower panel). (B) SPFM images of cells pre-stained with lysosomal marker: Dextran-FITC followed the incubation with 1.0 μM **1a** or **2a** for 24 h. SP NIR fluorescence is displayed in red, FITC fluorescence is displayed in green, nuclei stained by DAPI are displayed in blue. Bar: 25 μm.

solution. As far as we know, **2a** is the first fluorophore that possesses the capability to visualize the physiological events with both SP NIR fluorescence and TP deep red fluorescence.

In vitro fluorescence microscopic studies

Tolerable cytotoxicity is a pre-requirement for the clinical translation of a fluorophore. To address this issue, cell viabilities of **2a** and **1a** (control fluorophore) were tested in human epithelial cervical cancer HeLa cells *via* MTT assay. Fig. S4† shows the viabilities of HeLa cells after treatment with a series concentration of fluorophores for 24 h. Interestingly, the replacement of sulfates by carboxylate acids in carbon chain terminals significantly reduced the cytotoxicity of fluorophore. IC_{50} value of **2a** was measured as 140 μM that is about 3.5 times higher than that of **1a**. The above experimental results indicate the tolerable cytotoxicity of **2a**, which benefits its applications under *in vitro* as well as *in vivo* conditions. Subsequently, the cellular uptakes of **1a** and **2a** were evaluated by SPFM in HeLa cells (Fig. 3A). SPFM images showed that both fluorophores can be effectively taken up by HeLa cells, and these fluorophores predominately located in the perinuclear region as vesicular structures after treatment for 24 h. Previous reports demonstrated the lysosomal delivery of the cyanine derivatives in cancer cells.[29–31] To determine the subcellular location of the fluorophores, HeLa cells were pre-stained by lysosomal marker: Dextran-FITC, which was used as a long-term lysosomal fluorescence marker in live cells.[30] As shown in Fig. 3B, following the treatment of **1a** or **2a** for 24 h, both of them colocalized well with pre-stained

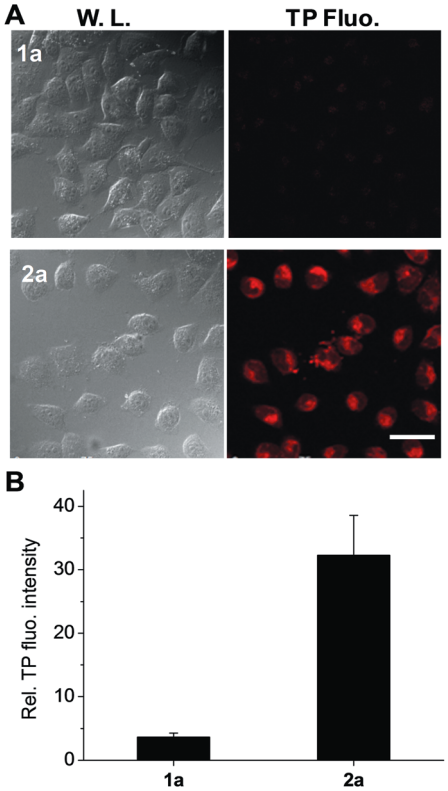

Fig. 4 Fluorophore **2a** internalized into live HeLa cells can be successfully visualized by TPFM after excitation at 900 nm. (A) White light (W. L.) and TPFM images of live cells upon incubation with **1a** (100 μM, upper panel) or **2a** (100 μM, lower panel) for 24 h. TP Fluo. signals were collected by the PMT channel ranging at 580–660 nm. Scale bar: 20 mm; (B) Mean cellular TP fluorescence intensities (with nearby background subtracted) after treatment of the fluorophore for 24 h. The values represent mean ± SD (n = 12).

lysosomes and the colocalization coefficient was calculated above 90% by using an Image J software with Pearson's plugin. The potential of **2a** as a TPFM fluorophore was further investigated in HeLa cells. Fig. 4A demonstrates the white light and TP fluorescence images of the cells treated with 100 μM **1a** or **2a** for 24 h upon excitation at 900 nm. While there was not any detectable TP intracellular fluorescence after treatment with **1a**, remarkable TP induced red fluorescence signals of **2a** were observed as vesicular structures in the perinuclear area. Quantification analysis showed that the average cellular TP fluorescence intensity of **2a** in a range of 580–660 nm was about 8.9 times higher than **1a** (Fig. 4B).

Conclusions

We developed a heptamethine cyanine based fluorophore that emits both SP NIR fluorescence and TP deep red fluorescence under physiological conditions. The advantages of this fluorophore, including tolerable cytotoxicity, high water solubility and strong single-photon/two-photon fluorescence, make it promising for intra-operatively optical image-guided tumor excision followed by TPFM biopsy analysis after a single administration. Additionally, the high lysosomal specificity of this fluorophore

makes it a potential candidate to detect aberrant lysosomal tracking and eventually develop to a new probe for studying lysosome-related diseases.

Acknowledgements

This work was supported by the National Basic Research Program of China (973 Program, No. 2011CB910404), National Natural Science Foundation of China (Nos. 81171384, 30900353, 30830039) and Shenzhen Bio-industry Development Fund-Basic Research Program (JC201005280607A).

Notes and references

1 Q. T. Nguyen, E. S. Olson, T. A. Aguilera, T. Jiang, M. Scadeng, L. G. Ellies and R. Y. Tsien, *Proc. Natl. Acad. Sci. U. S. A.*, 2010, **107**, 4317–4322.
2 G. M. van Dam, G. Themelis, L. M. A. Crane, N. J. Harlaar, R. G. Pleijhuis, W. Kelder, A. Sarantopoulos, J. S. de Jong, H. J. G. Arts, A. G. J. van der Zee, J. Bart, P. S. Low and V. Ntziachristos, *Nat. Med.*, 2011, **17**, 1315–1320.
3 I. D. Nagtegaal and P. Quirke, *J. Clin. Oncol.*, 2008, **26**, 303–312.
4 J. T. Huse and E. C. Holland, *Nat. Rev. Cancer*, 2010, **10**, 319–331.
5 S. Keereweer, J. D. Kerrebijn, P. B. van Driel, B. Xie, E. L. Kaijzel, T. J. Snoeks, I. Que, M. Hutteman, J. R. van der Vorst, J. S. Mieog, A. L. Vahrmeijer, C. J. van de Velde, R. J. Baatenburg de Jong and C. W. Lowik, *Mol. Imaging Biol.*, 2011, **13**, 199–207.
6 S. Gioux, H. S. Choi and J. V. Frangioni, *Mol. Imaging*, 2010, **9**, 237–255.
7 S. A. Hilderbrand and R. Weissleder, *Curr. Opin. Chem. Biol.*, 2010, **14**, 71–79.
8 E. S. Olson, T. Jiang, T. A. Aguilera, Q. T. Nguyen, L. G. Ellies, M. Scadeng and R. Y. Tsien, *Proc. Natl. Acad. Sci. U. S. A.*, 2010, **107**, 4311–4316.
9 H. Kobayashi, M. Ogawa, R. Alford, P. L. Choyke and Y. Urano, *Chem. Rev.*, 2010, **110**, 2620–2640.
10 L. Wang and C. Li, *J. Mater. Chem.*, 2011, **21**, 15862–15871.
11 R. Sharma, J. A. Wendt, J. C. Rasmussen, K. E. Adams, M. V. Marshall and E. M. Sevick-Muraca, *Ann. N. Y. Acad. Sci.*, 2008, **1131**, 13–36.
12 R. Weissleder, *Nat. Biotechnol.*, 2001, **19**, 316–317.
13 M. Fernandez-Suarez and A. Y. Ting, *Nat. Rev. Mol. Cell Biol.*, 2008, **9**, 929–943.
14 H. M. Kim and B. R. Cho, *Acc. Chem. Res.*, 2009, **42**, 863–872.
15 S. Luo, E. Zhang, Y. Su, T. Cheng and C. Shi, *Biomaterials*, 2011, **32**, 7127–7138.
16 M. Ogawa, N. Kosaka, P. L. Choyke and H. Kobayashi, *Cancer Res.*, 2009, **69**, 1268–1272.
17 Z. Zhang and S. Achilefu, *Chem. Commun.*, 2005, 5887–5889.
18 K. Kiyose, H. Kojima, Y. Urano and T. Nagano, *J. Am. Chem. Soc.*, 2006, **128**, 6548–6549.
19 F. Yu, P. Li, G. Li, G. Zhao, T. Chu and K. Han, *J. Am. Chem. Soc.*, 2011, **133**, 11030–11033.
20 D. Oushiki, H. Kojima, T. Terai, M. Arita, K. Hanaoka, Y. Urano and T. Nagano, *J. Am. Chem. Soc.*, 2010, **132**, 2795–2801.
21 A. Faust, B. Waschkau, J. Waldeck, C. Holtke, H. J. Breyholz, S. Wagner, K. Kopka, W. Heindel, M. Schafers and C. Bremer, *Bioconjugate Chem.*, 2008, **19**, 1001–1008.
22 R. C. Benson and H. A. Kues, *J. Chem. Eng. Data*, 1977, **22**, 379–383.
23 M. Ogawa, N. Kosaka, P. L. Choyke and H. Kobayashi, *ACS Chem. Biol.*, 2009, **4**, 535–546.
24 S. R. Mujumdar, R. B. Mujumdar, C. M. Grant and A. S. Waggoner, *Bioconjugate Chem.*, 1996, **7**, 356–362.
25 K. Kikuchi, M. Hoshi, T. Niwa, Y. Takahashi and T. Miyashi, *J. Phys. Chem.*, 1991, **95**, 38–42.
26 U. Rosch, S. Yao, R. Wortmann and F. Wurthner, *Angew. Chem., Int. Ed.*, 2006, **45**, 7026–7030.
27 S. Yazdanfar, C. Joo, C. Zhan, M. Y. Berezin, W. J. Akers and S. Achilefu, *J. Biomed. Opt.*, 2010, **15**, 030505.
28 M. Y. Berezin, C. Zhan, H. Lee, C. Joo, W. J. Akers, S. Yazdanfar and S. Achilefu, *J. Phys. Chem. B*, 2011, **115**, 11530–11535.
29 X. Yang, C. Shi, R. Tong, W. Qian, H. E. Zhau, R. Wang, G. Zhu, J. Cheng, V. W. Yang, T. Cheng, M. Henary, L. Strekowski and L. W. Chung, *Clin. Cancer Res.*, 2010, **16**, 2833–2844.
30 C. Li, T. R. Greenwood and K. Glunde, *Neoplasia*, 2008, **10**, 389–398.
31 C. Li, T. R. Greenwood, Z. M. Bhujwalla and K. Glunde, *Org. Lett.*, 2006, **8**, 3623–3626.

